

## Improving the accuracy of flood forecasting with transpositions of ensemble NWP rainfall fields considering orographic effects

Wansik Yu <sup>a,\*</sup>, Eiichi Nakakita <sup>b</sup>, Sunmin Kim <sup>c</sup>, Kosei Yamaguchi <sup>b</sup>

<sup>a</sup> International Water Resources Research Institute, Chungnam National University, Daejeon, Republic of Korea

<sup>b</sup> Disaster Prevention Research Institute, Kyoto University, Kyoto, Japan

<sup>c</sup> Department of Civil and Earth Resources Engineering, Kyoto University, Kyoto, Japan



### ARTICLE INFO

#### Article history:

Received 20 October 2015

Received in revised form 17 March 2016

Accepted 21 May 2016

Available online 28 May 2016

This manuscript was handled by Konstantine P. Georgakakos, Editor-in-Chief, with the assistance of Alan Seed, Associate Editor

#### Keywords:

Ensemble NWP rainfall

Flood forecasting

Transposition

Orographic rainfall

### SUMMARY

The use of meteorological ensembles to produce sets of hydrological predictions increased the capability to issue flood warnings. However, space scale of the hydrological domain is still much finer than meteorological model, and NWP models have challenges with displacement. The main objective of this study to enhance the transposition method proposed in Yu et al. (2014) and to suggest the post-processing ensemble flood forecasting method for the real-time updating and the accuracy improvement of flood forecasts that considers the separation of the orographic rainfall and the correction of misplaced rain distributions using additional ensemble information through the transposition of rain distributions. In the first step of the proposed method, ensemble forecast rainfalls from a numerical weather prediction (NWP) model are separated into orographic and non-orographic rainfall fields using atmospheric variables and the extraction of topographic effect. Then the non-orographic rainfall fields are examined by the transposition scheme to produce additional ensemble information and new ensemble NWP rainfall fields are calculated by recombining the transposition results of non-orographic rain fields with separated orographic rainfall fields for a generation of place-corrected ensemble information. Then, the additional ensemble information is applied into a hydrologic model for post-flood forecasting with a 6-h interval. The newly proposed method has a clear advantage to improve the accuracy of mean value of ensemble flood forecasting. Our study is carried out and verified using the largest flood event by typhoon 'Talas' of 2011 over the two catchments, which are Futatsuno (356.1 km<sup>2</sup>) and Nanairo (182.1 km<sup>2</sup>) dam catchments of Shingu river basin (2360 km<sup>2</sup>), which is located in the Kii peninsula, Japan.

© 2016 Elsevier B.V. All rights reserved.

## 1. Introduction

The accuracy of weather forecasts has steadily improved over the years, due to advances in numerical weather prediction (NWP) techniques and increased computing power. These NWP models represent the atmosphere as a dynamic fluid, solve for its behavior through the use of mechanics and thermodynamics, and use current weather conditions as input to atmospheric models to predict the evolution of weather systems (Golding, 2009; Cuo et al., 2011).

However, meteorological forecasting is difficult because the atmosphere is a nonlinear and chaotic system (Lorenz, 1969). A slight change in the initial and boundary layer conditions of a circulation system could result in unpredictable outcomes. Presently, one of the main alternatives is an ensemble NWP system with var-

ious initial and boundary conditions. It is believed that ensemble NWP systems exhibit greater forecast skill than any single NWP model control run or deterministic model run (e.g. Buizza et al., 1999; Demeritt et al., 2007). These recent advances in weather measurement and forecasting have created opportunities to improve flood forecasts.

At the same time, operational and research flood forecasting systems are increasingly moving toward using NWP model ensembles, known as ensemble prediction systems (EPSs), rather than single deterministic forecasts. EPSs in flood forecasting are now widely regarded as the state-of-the-art technique in forecasting science, following on the success of the use of ensembles for weather forecasting (e.g. Buizza et al., 2005; Gneiting and Raftery, 2005). EPSs have been used to account for uncertainties and make an attractive product for flood forecasting systems with the potential to extend lead time and better quantify predictability than any single deterministic run for the same location and time (Palmer and Buizza, 2007). As discussed by Seo et al. (2014), the

\* Corresponding author. Tel.: +82 42 821 7745; fax: +82 42 821 8957.

E-mail address: [yuwansik@gmail.com](mailto:yuwansik@gmail.com) (W. Yu).

recent researches on flood forecasting have been utilized and investigated EPSs and have found that ensemble forecasts in hydrological fields increase accuracy and allow for skillful predictions with extended lead time (e.g. [Xuan et al., 2009](#); [Roulin and Vannitsem, 2005](#); [Yu et al., 2014, 2015](#); [Fan et al., 2014](#); [Noh et al., 2014](#)).

However, in many cases, the potential of flood forecasting with EPS is described alongside cautious notes regarding variability and uncertainty of ensemble information. Several authors agreed that, compared to traditional deterministic forecasting, the additional information provided by EPS should help improve forecasting quality and provide flood forecasts with valuable information, but were less clear about exactly what that information was or how useful it might be for their operational purposes ([Palmer, 2002](#); [Legg and Mylne, 2004](#); [Hlavcova et al., 2006](#)). And, in some cases of medium-range meteorological forecasts, ensemble gave a clear flood signal up to 4 days in advance, but it has a restricted application for using EPSs effectively in flood forecasting systems on a small catchment scale because it needs localized higher accuracy in terms of rainfall prediction. As a result, EPSs with NWP models do not capture true rainfall distributions, in some cases, for short-range flood forecasting on a small catchment scale.

EPSs with NWP models also have challenges with misplacement of spatial rain distributions, which means the intensity and shape of a rainfall pattern may be correct but the location of spatial storm distribution deviates from the true rainfall distributions. As a result, the misplacement of rain distributions demonstrates the poor reliability of quantitative precipitation forecasts. [Schaake et al. \(2004\)](#) analyzed the statistical properties of the prediction outcomes from the US National Centers for Environmental Prediction (NCEP) during 1997 and 1999 over the continental US. They found that ensemble forecasts were biased in many cases and the ensemble spread was insufficient to capture the forecast error distribution. [Ebert and McBride \(2000\)](#) also stated that QPF quality needs to be improved in order to provide reliable hydrologic prediction, and errors in location misplacement, timing, and intensity hampered the direct application of QPF from the NWP into hydrologic prediction models. In order to use EPSs properly into flood forecasting systems on a small catchment scale, above mentioned meteorological characteristics (e.g. spatial shift, and rather coarse resolution yet) should be considered carefully.

Given the current issue and problem with EPSs with NWP models, a proper pre-processing dealt with spatial misplacement of rainfall distributions should be considered carefully, in order to use EPSs effectively in flood forecasting systems on a small catchment scale. [Yu et al. \(2014\)](#) have utilized and investigated this ensemble NWP rainfall forecast for flood forecasting and proposed a spatial shift (hereafter, transposition) of ensemble rain distributions to improve the accuracy of flood forecasts. However, in cases of the transposition of rain distributions in mountainous areas, the problem arises that the orographic rain patterns also move to non-mountain areas with the transposition scheme. As a result, it results in a great loss of the physical meaning of orographic rainfall. To prevent the problem of orographic rainfall shifting, we modified [Yu et al.'s \(2014\)](#) method of separating ensemble NWP rainfalls into orographic and non-orographic rain fields by solving physically based equations that included the atmospheric variables in advance of the transposition scheme.

The aim of this research is to suggest the post-processing ensemble flood forecasting method for the real-time updating and the accuracy improvement of flood forecasts that considers two points: the separation of the orographic rainfall and the correction of misplaced rain distributions using additional ensemble information through the transposition of rain distributions. [Fig. 1](#) shows a flowchart of the proposed process in this study for the real-time updating of flood forecasts using transposition of rainfall

fields that considers orographic rainfall. The newly proposed method is comprised of 5 steps. The first step is the separation of ensemble NWP rainfalls into orographic and non-orographic rain fields using the extraction of topography effect. Then, the non-orographic rainfall fields are examined by the transposition scheme to produce additional ensemble information (step 2), and ensemble NWP rainfall fields are calculated by recombining the transposition results of non-orographic rain fields with those of orographic rainfall fields in order to generate place-corrected ensemble information (step 3). The recombined ensemble rain fields are spatially verified by C-band composite radar data from the Ministry of Land, Infrastructure, Transport and Tourism (MLIT) of Japan for the previous 6 h with error indexes—namely, the critical success index (CSI) and the root mean square error (RMSE)—to find out the appropriate ensembles and transposed locations (step 4). The best ensemble members and transposed locations give information to hydrologic models for real-time updating of post-flood forecasting within a 6-h interval (Step 5) in the Typhoon Talas event of 2011.

This article has been organized in the following way. After the introduction, Section 2 introduces the design of meteorological experiment for the Typhoon Talas event, and Section 3 describes a hydrologic model, and target area. Section 4 suggests the methodology for the calculation of orographic effect and transposition scheme for making ensemble information. Section 5 addresses the results of transposition considering misplaced spatial location and real-time updating of flood forecasting, and finally, we summarize our major conclusions in Section 6.

## 2. Meteorological experiment

In early September 2011, heavy rainfalls happened over Japan due to season's 12th typhoon Talas. Typhoon Talas was an unusually large tropical cyclone that caused many deaths and severe damage to Japan. It was the 7th severe tropical storm of the 2011 Pacific typhoon season. Throughout Japan, Talas brought heavy rainfall leaving roads flooded. It also caused unprecedented human damage, resulting in 78 dead and 16 missing. Talas moved very slowly and had a huge gale diameter throughout its life. The total amount of precipitation from Talas in the Kii Peninsula was estimated to be over 2000 mm.

In the present study, JMA's Non-Hydrostatic Model (NHM, [Saito et al., 2006](#); [Saito, 2012](#)) has been experimentally conducted by the Meteorological Research Institute (MRI) of JMA for the ensemble forecast of typhoon Talas event that occurred over Kinki area in Japan in September 2011. The ensemble forecast systems are composed of 11 members (1 unperturbed and 10 perturbed members) with a horizontal resolution of 10 km and 2 km, which is later nested inside the former with a 6-h lag.

The domain of coarse resolution of 10 km was carried out over Japan area (D01 in [Fig. 2](#)), and had a domain of  $361 \times 289$  grid points with 50 vertical levels, forecasted up to 36 h. For initial and lateral boundary conditions, 10 km used the analysis from the JMA non-hydrostatic 4DVAR (JNoVA) data assimilation system ([Honda and Sawada, 2008](#)) and the forecasts of JMA's high-resolution (TL959L60) global spectral model (GSM). The NHM contains a modified Kain-Fritsch convective parameterization scheme along with 3 ice bulk cloud microphysics ([Lin et al., 1983](#)). The control run (cntl) is the forecast with a non-perturbed analysis, and the 10 perturbed forecasts were generated from JMA's 1-week global EPS (WEP) for the initial and boundary perturbations.

In order to focus on the quantitative precipitation forecast of the severe rainfall event, the nested downscale forecast was executed with a higher resolution of 2 km with a 6-h lag from 10 km resolution forecast. The fine resolution system had a domain of

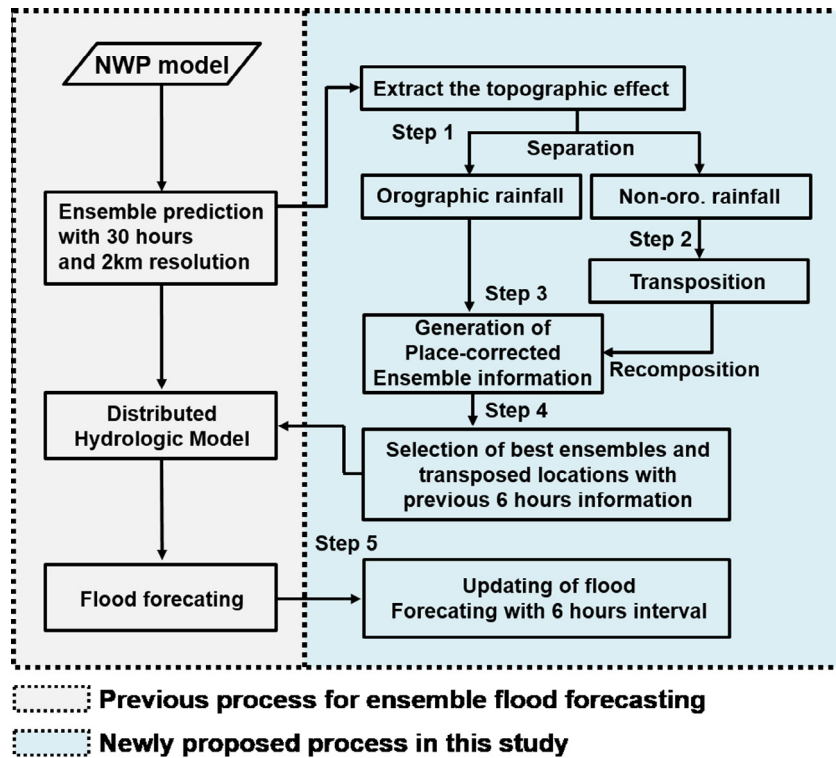


**Fig. 1.** Flowchart of the proposed process for the real-time updating of flood forecasting using transposition of ensemble NWP rainfall fields considering orographic rainfall.

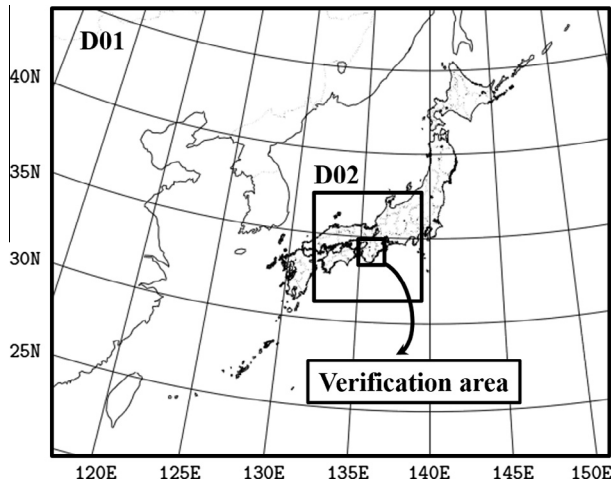


**Fig. 2.** Forecast domains of 10 km (D01) and 2 km (D02) horizontal resolution. The rectangle inside 2 km domain denotes the verification area.

350 × 350 grid points with 60 vertical levels (D02 in Fig. 2), and forecasted up to 30 h. The initial and boundary condition for each member in 2 km were interpolated from the forecasts on the corresponding member in 10 km resolution with a 6-h lag. The 2 km resolution forecast did not use a convective scheme because of its cloud resolving resolutions. The domain of the two ensemble systems with 10 km and 2 km horizontal resolution are illustrated in Fig. 2.

In this study, we introduced the results of ensemble prediction with a 2 km horizontal resolution due to the viewpoints of high resolution and better predictability of weather phenomena (Yu et al., 2015), and used 2 sets of ensemble prediction outputs with 30 h forecast time to assess the proposed method for the flood

forecast using transposition of ensemble NWP rainfall fields considering orographic effects (Table 1).

### 3. Study area and a hydrologic model

#### 3.1. Study area

The proposed methods are applied to the Shingu river basin, which is located in Japan, to compare flood forecast accuracy utilizing the original ensemble NWP rainfall with the results of transposition scheme of spatial rainfall fields as illustrated in Fig. 3. The Shingu river Basin is located in the Kii Peninsula of the Kinki area, Japan and covers an area of 2360 km<sup>2</sup>. The average elevation of the study site is 644.6 m, and the slope is steep; this basin is a mountainous area. The five dams, Futatsuno, Kazeya, Komori, Nanairo, and Ikehara are located upstream. Of the five dam catchments, we focused on two sub-catchments, which are Futatsuno (356.1 km<sup>2</sup>) and Nanairo (182.1 km<sup>2</sup>) dam catchments (Nos. 1 and 4 of Fig. 3), to improve the accuracy of the flood forecasting in small catchments. Two additional dams, Kazeya and Ikehara (Nos. 2 and 5 of Fig. 3), are located upstream of the Futatsuno and Nanairo catchments, respectively. Here, the observed outflows from the Kazeya and Ikehara dam were directly utilized as the upper boundary conditions for the subject dam basins to focus on only the Futatsuno and the Nanairo catchments.

#### 3.2. A hydrologic model

The applied hydrologic model is a spatially-distributed hydrologic model, and one-dimensional kinematic wave method for subsurface and surface flow (hereafter, KWMSS) with a conceptual stage-discharge relationship for the Shingu river basin based on two element modules: a hillslope runoff generation module, a river routing module. The drainage network is represented by sets of

**Table 1**

Two forecast sets with 30 h forecast time and 2 km horizontal resolution used in the study. Each forecast is overlapped with 6 h.

Forecast period	1st forecast	2011/09/02 03:00 – 09/03 09:00 JST (30 h)
	2nd forecast	2011/09/03 03:00 – 09/04 09:00 JST (30 h)

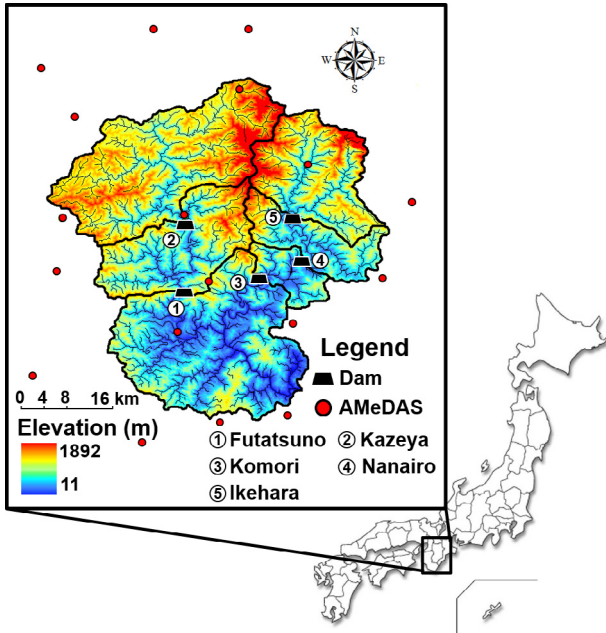


**Fig. 3.** Shingu river basin, which is target area within Kii Peninsula in Japan.

hillslope and channel elements from digital elevation model (DEM), and was represented by a 250 m × 250 m spatial resolution of DEM. The hillslope and river routing modules were developed as elements of a distributed hydrological model using the kinematic wave theory in a previous study (Tachikawa et al., 2004). In this model, it is considered that the catchment consists of a number of rectangular slope elements which drain to the steepest gradient of its surroundings, as shown in Fig. 4. The rainfall over all hillslope elements flows one-dimensionally into the river nodes and then routes to the catchment outlet. The rainfall–runoff transformation

conducted by KWMSS is based on the assumption that each hill-slope element is covered with a permeable soil layer. In these conceptual soil layers, slow and quick flow are simulated as unsaturated Darcy flow and saturated Darcy flow, respectively, and overland flow occurs if water depth,  $h$  [m] exceeds soil water capacity. The flow rate of each hillslope element  $q$  [m<sup>2</sup>/s] is calculated by Eq. (1), and combined with the continuity equation for channel routing by Eq. (2). The KWMSS model has been applied to several catchments in Japan and Korea with different climatic and geographic conditions (Sayama et al., 2006; Kim et al., 2009; Lee et al., 2013; Yu et al., 2015).

$$q = \begin{cases} v_c d_c (h/d_c)^\beta, & 0 \leq h \leq d_c \\ v_c d_c + v_a (h - d_c), & d_c \leq h \leq d_s \\ v_c d_c + v_a (h - d_c) + \alpha (h - d_s)^m, & d_s \leq h \end{cases} \quad (1)$$

$$\frac{\partial h}{\partial t} + \frac{\partial q}{\partial x} = r(x, t) \quad (2)$$

where  $v_c = k_c i$  [m/s],  $v_a = k_a i$  [m/s],  $k_c = k_a/\beta$  [m/s],  $\alpha = i^{1/2}/n$  [m<sup>1/3</sup> s<sup>-1</sup>],  $m = 5/3$ ,  $i$  is the slope gradient,  $k_c$  [m/s] is the hydraulic conductivity of the capillary soil layer,  $k_a$  [m/s] is the hydraulic conductivity of the non-capillary soil layer,  $n$  [m<sup>-1/3</sup> s] is the roughness coefficient,  $d_s$  [m] is the water depth corresponding to the water content, and  $d_c$  [m] is the water depth corresponding to maximum water content in the capillary pore.

## 4. Methodology

### 4.1. Physically-based method for orographic rainfall

Orographic rainfall supplies mountain glaciers and rivers and provides water for irrigation, hydropower, and human consumption (Smith et al., 2008). Orographic effects on atmospheric flow can produce or modify precipitating clouds through orographic lifting, triggering of convection, indirect effects of flow splitting or blocking, and induced waves. Many examples of orographic precipitation have been studied over last 50 years, and various simplified conceptual mechanisms have been proposed to evaluate observations (e.g. Smith, 1979, 2006; Banta, 1990; Smith et al., 2008; Houze, 2012). There are different mechanisms of orographic rainfall (e.g. stable upslope ascent, seeder-feeder mechanism, partial blocking of the impinging air mass, down-valley flow induced by evaporative cooling etc.). The most straightforward mechanism of orographic rainfall is stable upslope ascent: Forced mechanical lifting of the air impinging on the windward flank leads to cooling of the air column, resulting in condensation and precipitation; descent in the lee leads to warming and drying, and precipitation is suppressed (Roe, 2005). Another effect is the “seeder-feeder” mechanism according to which precipitating hydrometeors that originate from a cloud layer aloft (the “seeder” cloud) grow at the expense of the water content of a cloud below (the “feeder” cloud). Falling precipitation from the seeder cloud accretes additional moisture when it falls through the feeder cloud, either by coalescence or by riming, and so precipitation is increased over the hill (e.g., Tatehira, 1976; Bader and Roach, 1977; Hill et al., 1981; Robichaud and Austin, 1988; Roe, 2005).

Tatehira (1976) proposed a physically-based method for calculating orographic and non-orographic rainfall fields from observed radar rainfall measurements. Many studies have applied and verified this method in a variety of hydrologic applications, and have shown that this method was effective and adequate to consider the orographic and non-orographic rainfall (Nakakita and Terazono, 2008; Nakakita et al., 2012). However, they used the radar rainfall measurements to separate the orographic and non-orographic rainfall in previous study, whereas our approach applies

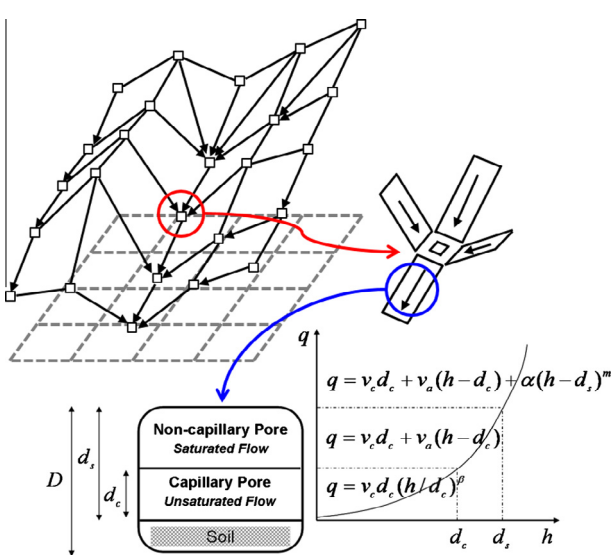


**Fig. 4.** Conceptualization of spatial flow movement and flow process in the hillslope model.

this method into the ensemble NWP rainfall as mentioned previously.

In this study, we used the physically-based method proposed by Tatehira (1976) for calculating orographic and non-orographic rainfall fields. In this method, the orographic effect is calculated based on the seeder-feeder mechanism. In other words, non-orographic hydrometeors are produced in upper layers, and the hydrometeors capture cloud droplets produced by the orographic effect in low layers. The precipitation droplets or ice particles fall from an upper-level precipitating cloud (seeder) and collect cloud water as they pass through a lower-level orographic stratus cloud (feeder) by collision and coalescence, thus producing greater precipitation on the mountainous area under the cap cloud than on the nearby flat regions. The availability of the process depends on sufficiently strong low-level moist flow to maintain the cloud water content in the orographic feeder cloud and the continuing effectiveness of precipitation particles from the seeder cloud.

The strong rain-bands stagnated near the mountain top (orographic rainfall) are estimated using additional atmospheric variables. The flux of cloud water content  $L$  ( $\text{g/m}^3$ ) in rising air parcel along with a wind is calculated by Eq. (3) (Tatehira, 1976; Nakakita and Terazono, 2008; Nakakita et al., 2012).

$$\frac{dL}{dt} = -cL - a(L - L_c) + WG - WL \left( \frac{\partial \ln \rho_v}{\partial z} \right) \quad (3)$$

where  $\rho_v$  is the density of water vapor ( $\text{g/m}^3$ ),  $c$  is the ratio of cloud drops captured by seeder hydrometeors of an upper-level,  $a$  is the ratio of precipitation particles to cloud drops,  $L_c$  is the threshold amount of water content before conversion into precipitation ( $\text{g/m}^3$ ) and  $G$  is the amount of saturated water vapor  $\rho_s$  increased by a rising saturated air parcel ( $\text{g/m}^4$ ) (i.e.  $-d\rho_s/dz$ ). Finally,  $W$  is the vertical wind velocity ( $\text{m/s}$ ), which is estimated by an inner product of horizontal wind and gradient of topographic height using DEM. In this study, we assumed that the cloud droplets of orographic cloud in low layers does not grow up in case of the negative value of  $dL/dt$  on downslope area.

These atmospheric variables (Air temperature, horizontal wind, relative humidity) are estimated by the use of Grid Point Value (GPV) data from Japan Meteorological Agency (JMA), and are solved in the seven layers at heights of 200, 400, 1000, 2000, 3000, 4000, and 5000 m in the  $\sigma$ -vertical coordinate system using the method of Nakakita et al. (1996). In Eq. (3), the first and second terms on the right-hand side are related with that the amount of water content is decreased. The third term shows the water vapor

condensing as the air parcel ascends with a unit distance. The last term expresses the influence of atmospheric compressibility, and can be ignored because the order of this term is less than other terms. The amounts of cloud water content in an inflow and outflow mesh ( $L_{in}$  and  $L_{out}$ ) can be calculated by the integral of Eq. (3) with respect to time  $t$ .

$$L_{out} = \frac{WG + aL_c}{c + a} + \left( L_{in} - \frac{WG + aL_c}{c + a} \right) e^{-(c+a)\Delta t} \quad (4)$$

In this study, the ensemble NWP rainfall  $R_{NWP}$  is interpreted to be the summation of orographic rainfall  $R_o$  and non-orographic rainfall  $R_n$  (Eq. (5)). Nakakita and Terazono (2008) suggested the Eq. (6) for orographic rainfall intensity  $R_o$  ( $\text{mm/h}$ ) and assumed that the ratio  $c$  of cloud drops captured by raindrops is estimated by Eq. (7). Finally, the orographic rainfall is supposed to be a function of non-orographic rainfall and is calculated by solving the simultaneous Eqs. (4)–(7) in multi-atmospheric layers.

$$R_{NWP} = R_o + R_n \quad (5)$$

$$R_o = \frac{L_{in} + WG\Delta t - L_{out}}{\Delta t} \times 3.6 \times H \quad (6)$$

$$c = 0.6778 R_n^{0.731} \times 10^{-3} \quad (7)$$

where  $L_{in}$  and  $L_{out}$  are amounts of cloud water content ( $\text{g/m}^3$ ) in an inflow and outflow side mesh, respectively.  $\Delta t$  is a timescale (s) during an air parcel passes one mesh, and  $H$  is the thickness of each layer (m).

Fig. 5 shows the procedure for the separation of orographic and non-orographic rainfall. First, cloud water content is calculated from atmospheric variables of grid mesh in each layer vertically, and the ensemble NWP rainfall ( $R_{NWP}$ ) is assumed to be that of the lowest layer (200 m height). It is separated into orographic ( $R_{o1}$ ) and non-orographic ( $R_{n1}$ ) rainfall by solving equations of (4)–(7). It is supposed that the non-orographic rainfall ( $R_{n1}$ ) is expressed as the sum of the orographic rainfall ( $R_{o2}$ ) and non-orographic rainfall ( $R_{n2}$ ) in the upper layer. In this way, orographic rainfall and non-orographic rainfall of each layer can be separated from the lowest to the highest layer repeatedly. Then the non-orographic rainfall field of highest layer is utilized as an input domain for the transposition scheme to make additional ensemble information. And total orographic rainfall in each layer gives the value by recombining the transposition results of non-orographic rainfall field.

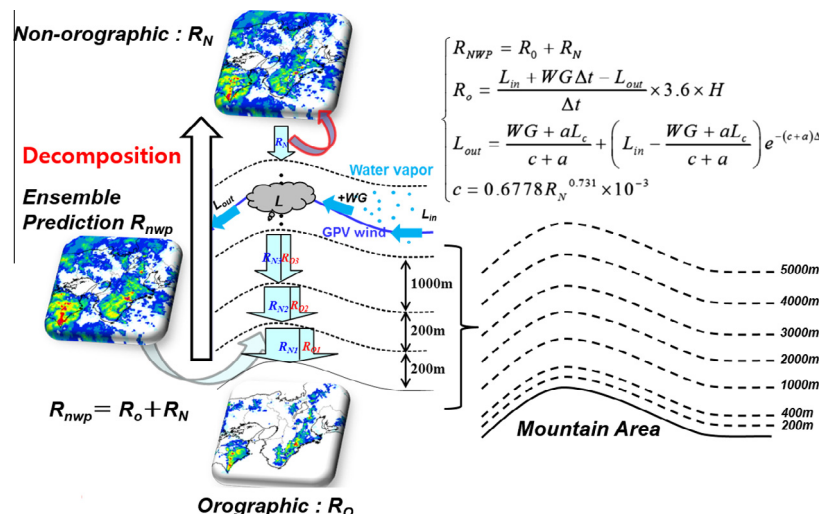
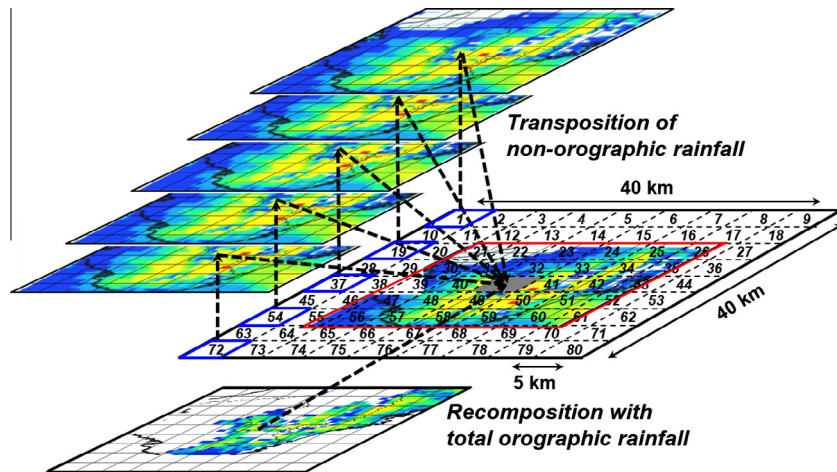


Fig. 5. Procedure for a calculation of orographic and non-orographic rainfall.



**Fig. 6.** A schematic of transposition scheme using non-orographic rainfall fields, and recombining with the total orographic rainfall in each vertical layer.

#### 4.2. Transposition of non-orographic rainfall field

As previously stated, we examined the transposition scheme of non-orographic rainfall field in order to produce additional ensemble information and consider the misplacement from the original spatial position. Many EPSs are based on a Monte Carlo framework of NWP model with one realization starting from a central analysis (the control forecast) and others generated by perturbing the initial and/or boundary conditions (the perturbed forecasts) (Cloke and Pappenberger, 2009). In this study, we also used ensemble NWP rainfall created by perturbation of initial and boundary conditions, and we took into consideration the transposition scheme for more additional ensembles. The technique for making additional ensemble information is fairly straightforward in this study. We utilized spatial transposition of each separated non-orographic rain fields.

Fig. 6 shows a schematic of transposition scheme using non-orographic rainfall fields, and recombining with the total orographic rainfall in each vertical layer. For the transposition with separated non-orographic rainfall fields from the established ensemble prediction, the transposed catchment mask ( $100 \text{ km} \times 100 \text{ km}$ ) moved into the original forecast domain from location 1–80 with a maximum distance in the  $x$  and  $y$  directions of each at about 20 km with 5 km interval in order to produce additional ensemble information. We finally constructed additional 891 transposed ensemble domains (existing 11 ensemble members  $\times$  80 locations + 11 original locations of established ensemble members). The final place-corrected ensemble rainfall fields are estimated by integrating the transposed non-orographic rain fields with the total orographic rainfall, which is calculated in each vertical layer. Then we compared the place-corrected ensemble rainfall field with MLIT observed radar rainfall fields using critical success index (CSI) and root mean square error (RMSE) to examine the well-suited ensemble members and transposition locations during 6-h interval for the flood forecast updating. We considered the top 10% ensemble members and transposition locations, which have high efficiency criteria for each RMSE and CSI value, of each ensemble member during previous 6 h, in order to apply them to the flood forecasting after 6 h. The real-time updating of flood forecasts with a 6-h interval are based on the assumption that misplacement behaviors of rainfall distribution have continuity between previous 6 h and after 6 h of transposition locations.

#### 5. Results and discussion

In previous research, Yu et al. (2014) also have been utilized the transposition method to address the uncertainties in ensemble

hydrological forecasting and to improve an accuracy of flood forecasting. They investigated the appropriate transposed locations of ensemble rainfall fields during the current period to apply the transposed information into the next target period of flood forecasting, and evaluated the continuity of misplacement behavior of ensemble rainfall from the current period to the next target period. Our approach in this study agrees with that of Yu et al. (2014) in terms of the accuracy improvement of flood forecasting skill, but differs from previous approach in two main aspects. First is that our approach considered the separation of rainfall distribution into orographic and non-orographic rainfall. Second is that our approach took into account the transposed information with 6 h interval and applied to flood forecasting for real-time updating, whereas Yu et al. (2014) considered for 30 h of the current period to find out the appropriate transposed locations, and applied into 30 h of the next target period separately. Our approach in this paper mainly focuses on the real-time updating of the flood forecasting using transposed ensemble approach with 6 h interval.

#### 5.1. Decomposition of orographic rainfall

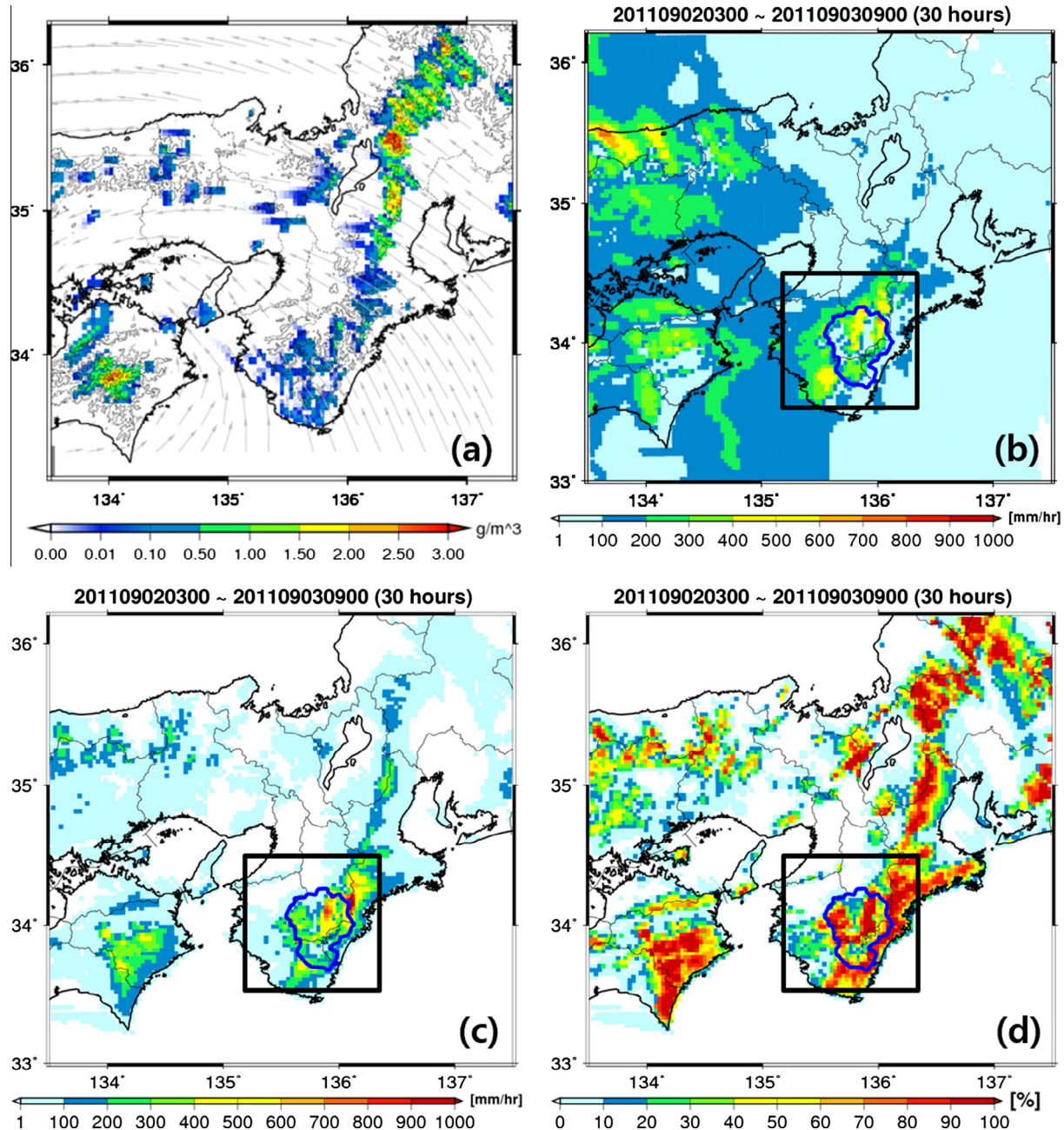
In this study, we separated the established 11 ensemble rainfall fields into orographic and non-orographic rainfall using physically-based method to take advantage of the non-orographic rainfall into transposition scheme for additional ensemble information. Based on the results of separated orographic and non-orographic rainfall, we investigated the orographic rainfall how comprised and dominant in total rainfall over the verification area of Fig. 2.

Fig. 7 shows the flux of cloud water content  $L(\text{g}/\text{m}^3)$  in rising air parcel along with a wind at a height of 400 m on 5:00 pm 3 September, the accumulated non-orographic and orographic rainfall by control run forecast, which is a non-perturbed analysis, and comprising proportion of accumulated orographic rainfall in total rainfall during 30 h of 1st forecast period. The comprising ratio of the orographic rainfall is calculated as follow.

$$\text{ratio}_{i,j} = \frac{R_{o,i,j}}{R_{\text{total},i,j}} \quad (8)$$

where  $R_{o,i,j}$  and  $R_{\text{total},i,j}$  are the accumulated orographic and total rainfall of each grid cell.

From Fig. 7, the mountainous regions are in agreement with the areas of orographic rainfall happened, and the orographic rainfall occurs considerably on the windward side of the mountain area. And note that there is an abundance of the non-orographic rainfall in non-mountainous area, whereas orographic rainfall was predominant in verification area which is mountainous region. And



**Fig. 7.** (a) Flux of cloud water content  $L$  ( $\text{g}/\text{m}^3$ ) in rising air parcel along with a wind at a height of 400 m on 5:00 pm 3 September, (b) accumulated non-orographic rainfall by control forecast, (c) accumulated orographic rainfall, and (d) comprising ratio of orographic rainfall in total rainfall. The rectangle inside domain denotes the verification area. The bold red line shows the Shingu river basin, which includes two sub-catchments of Futatsuno and Nanairo dam catchment.

the comprising ratio of the orographic rainfall in verification area exceeded over 50% and maximum percentage is 99.8%. From these results, it apparent that the orographic and non-orographic rainfall should be separated and just only non-orographic rain fields should be utilized for spatial transposition because the orographic rain patterns also move to non-mountain area with the transposition scheme if not separated.

We also visualized the orographic and non-orographic rainfall patterns separated from 11 established ensemble members with mean areal rain rates of the Shingu river basin during 54 h of two forecast periods. Fig. 8 shows comparisons of orographic (circle) and non-orographic (square) rainfall during the forecasted ensemble NWP rainfall in two forecast periods. Mean areal rain rates ( $\text{mm}/\text{h}$ ) over the Shingu river basin are shown in the plot. Each orographic and non-orographic rainfall comprised in ensem-

ble NWP rainfall is represented on the y-axis, respectively. Through Fig. 8, areal orographic rainfall rates are dominant over non-orographic rainfall until 20  $\text{mm}/\text{h}$  of ensemble NWP rain rate, whereas the component ratio of the orographic rainfall decreases with a two-dimensional trend line over 20  $\text{mm}/\text{h}$ . It means that the orographic rainfall in the total rainfall from light ( $0.1 \text{ mm}/\text{h}$ ) to intense ( $20 \text{ mm}/\text{h}$ ) of mountainous region is significant factor in the rainfall development, but the non-orographic rainfall had a component ratio higher than the orographic rainfall in case of the heavy rainfall over 20  $\text{mm}/\text{h}$ .

## 5.2. Transposition considering misplaced spatial location

We finally constructed 891 transposed ensemble domains by integrating the transposed non-orographic rain fields with the oro-

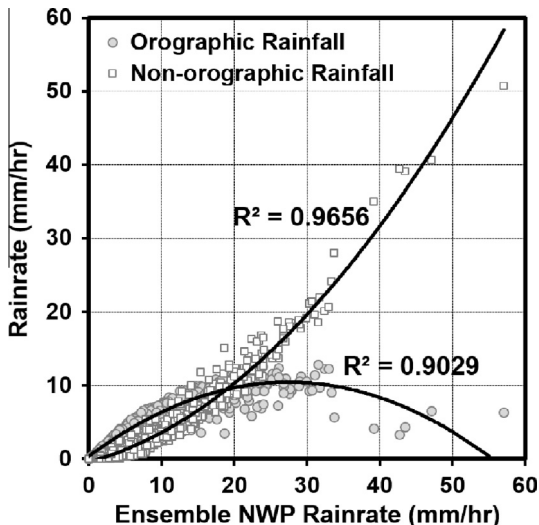


**Fig. 8.** Comparisons of orographic (circle) and non-orographic (square) rainfall during the two sets of forecast time of ensemble NWP rainfall. Mean areal rain rates (mm/h) over the Shingu river basin are shown in the plot.

graphic rain fields as stated in Section 4.2. Transposed ensemble domains have been verified spatially with MLIT observed radar rain data in the verification area to investigate the appropriate ensemble members and transposition locations, which have high efficiency criteria during previous 6 h interval for updating of flood forecasting. We used two popular indices to evaluate transposed ensemble domains: critical success index (CSI) for qualitative verification and root mean square error (RMSE) for quantitative verification, expressed as follows.

$$CSI = \frac{H}{H + M + FA} \quad (9)$$

$$RMSE = \sqrt{\frac{1}{N} \sum_{i,j=1}^N (O_{ij} - F_{ij})^2} \quad (10)$$

where  $N$  is the total grid cells ( $100 \times 100$ ) in verification area,  $O_{ij}$  and  $F_{ij}$  are the observed and forecasted rainfall of each grid cell at forecast time  $t$ ,  $H$  is the number of correct forecasts over the threshold (i.e., when the rainfall that is forecasted is also observed), and  $M$  is the number of times rainfall is not forecasted, but is observed.  $FA$  is the number of times rainfall is forecasted, but not observed.

For the calculation of CSI value, the ensemble forecasts were expressed as probabilities of exceeding a selected rainfall threshold (10 mm/h), which were used to compare an obvious spatial distribution of observed MLIT radar data with forecasted NWP rainfall. A contingency table can be constructed with a spatial comparison, in which each area with more than 10 mm/h of threshold is defined as “yes,” and other areas are defined as “no” for both forecasted and observed rainfall fields (Table 2).

Fig. 9 shows the results of the average CSI and RMSE from start point of original NWP rainfall to 6 h (From 0300 JST 2 September to 0900 JST 3 September 2011) in a comparison of observed radar rainfall and each transposed NWP rainfall domain during the 1st forecast period. Each grid value means the average CSI and RMSE when a transposed mask domain center with the each grid moved to an original domain with zero points of the  $x$  and  $y$  locations. Based on comparison of observed radar domain and each transposed outputs, most of CSI values provided a well-matched spatial pattern in case of transposition from central and left grid points to an original domain, whereas the member 1 and 5 were close to zero value in overall grid points, caused by the spatial shift of ensemble NWP rainfall from the correct spatial position. From

**Table 2**

A contingency table showing the frequencies of predicted and/or observed events determined by threshold ( $T$ ).

Observed	Predicted		
	Rain $< T$	Rain $> T$	Rain $> T$
	Zeroes (Z)	False alarms (FA)	Hits (H)

the CSI results of Fig. 9(a), the forecasted rainfall patterns moved slowly compared with real rainfall pattern, because the path direction of rainfall was from left to right direction. On the other hand, the RMSE value of Fig. 9(b) showed well-matched values in the middle areas of original domain. Fig. 10 also shows the results of the average CSI and RMSE from next 6 h of start point to 12 h (From 0900 JST 2 September to 1500 JST 3 September 2011). From the results of Figs. 9 and 10, we confirmed that spatial distribution patterns of the CSI and RMSE comparison results during the first 6 h and next 6 h were similar, and it can be said that misplacement behaviors of rainfall distribution have the continuity of transposition locations in each CSI and RMSE pattern.

As stated above, the real-time updating of flood forecasts with a 6-h interval starts with the assumption that misplacement behaviors of rainfall distribution have continuity between 0 and 6 h and from 6 to 12 h of transposition locations. Therefore, a verification measure using correlation coefficients was adopted to conduct a continuity assessment of misplacement behaviors of rainfall distribution with critical success index (CSI) in each 6-h update step. We considered the spatial CSI distribution, but not RMSE distribution to assess the spatial continuity because CSI measures the forecast accuracy in terms of the spatial distribution, whereas RMSE measures the quantitative accuracy. The correlation coefficient has been computed as follows:

$$corr = \frac{cov(A, B)}{\sigma_A \sigma_B} = \frac{N \sum_{i=1}^N A_i B_i - \sum_{i=1}^N A_i \sum_{i=1}^N B_i}{\sqrt{\left[ N \sum_{i=1}^N A_i^2 - \left( \sum_{i=1}^N A_i \right)^2 \right] \left[ N \sum_{i=1}^N B_i^2 - \left( \sum_{i=1}^N B_i \right)^2 \right]}} \quad (11)$$

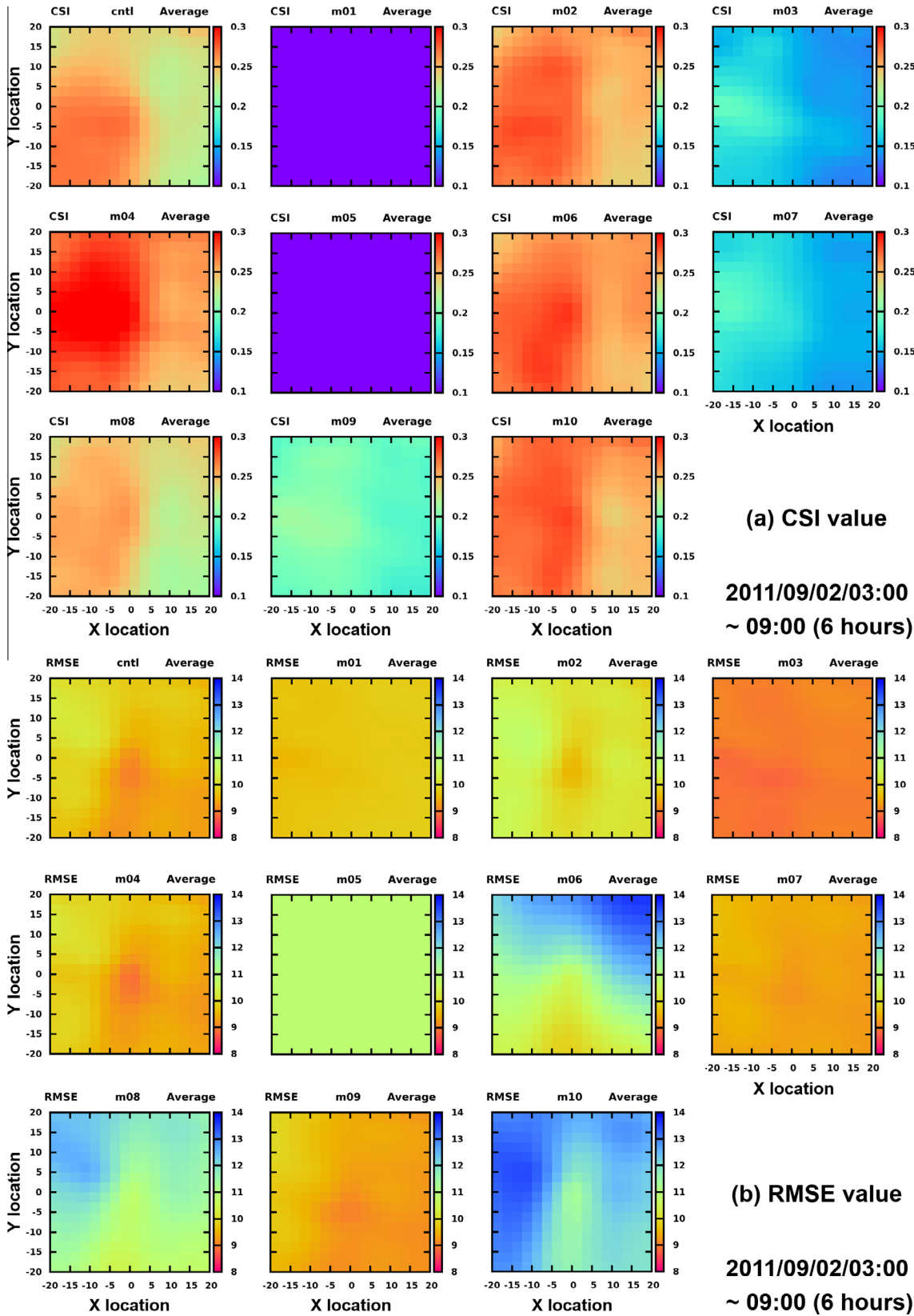
where  $A$  is the average CSI results of each ensemble member from 0 to 6 h (i.e., Fig. 9(a)),  $B$  represents the average CSI results of each ensemble member from 6 to 12 h (i.e., Fig. 10(a)),  $cov$  is the covariance of average CSI results between 0 to 6 h and 6 to 12 h of transposition locations, and  $\sigma_A$  and  $\sigma_B$  are the standard deviations of average CSI results from 0 to 6 h and from 6 to 12 h, respectively.

Table 3 shows the continuity assessment of transposition behaviors of forecasted rainfall distribution using the correlation coefficient of the critical success index (CSI) in each 6-h update step for real-time updating of flood forecasts, and the correlation coefficient with CSI distribution was recorded over 0.42–0.95. It means that the transposition scheme is continually satisfied during the two 6-h update steps and is appropriate for real-time updating of flood forecasts.

### 5.3. Real-time updating of post-flood forecasting

In this study, we considered the top 10% transposition locations, which have high efficiency criteria for each RMSE and CSI value, of a total 891 additional ensemble members during the 6-h interval (180 ensemble members; 90 members from CSI verification and 90 members from RMSE verification) in order to apply them to post-flood forecasting and assess the accuracy improvement for the application of real-time updating of flood forecasts.

The proposed approach has been tested in the Futatsuno and Nanairo dam catchments of the Shingu river basin for the real-



**Fig. 9.** Average CSI and RMSE results of 6 h (From 0300 JST 2 September to 0900 JST 3 September 2011) in a comparison of observed radar rainfall and each transposed NWP rainfall domain during the 1st forecast period.

time updating of flood forecasts for the largest flood event of 2011, which was caused by Typhoon Talas. Fig. 11 shows the ensemble flood forecasts using the original 11 ensemble members in 1st fore-

cast periods and corresponding post-flood forecasts after 6 and 12 h by transposition updating over the Futatsuno dam catchment. Fig. 11 illustrates a complete set of the forecasted discharge for the

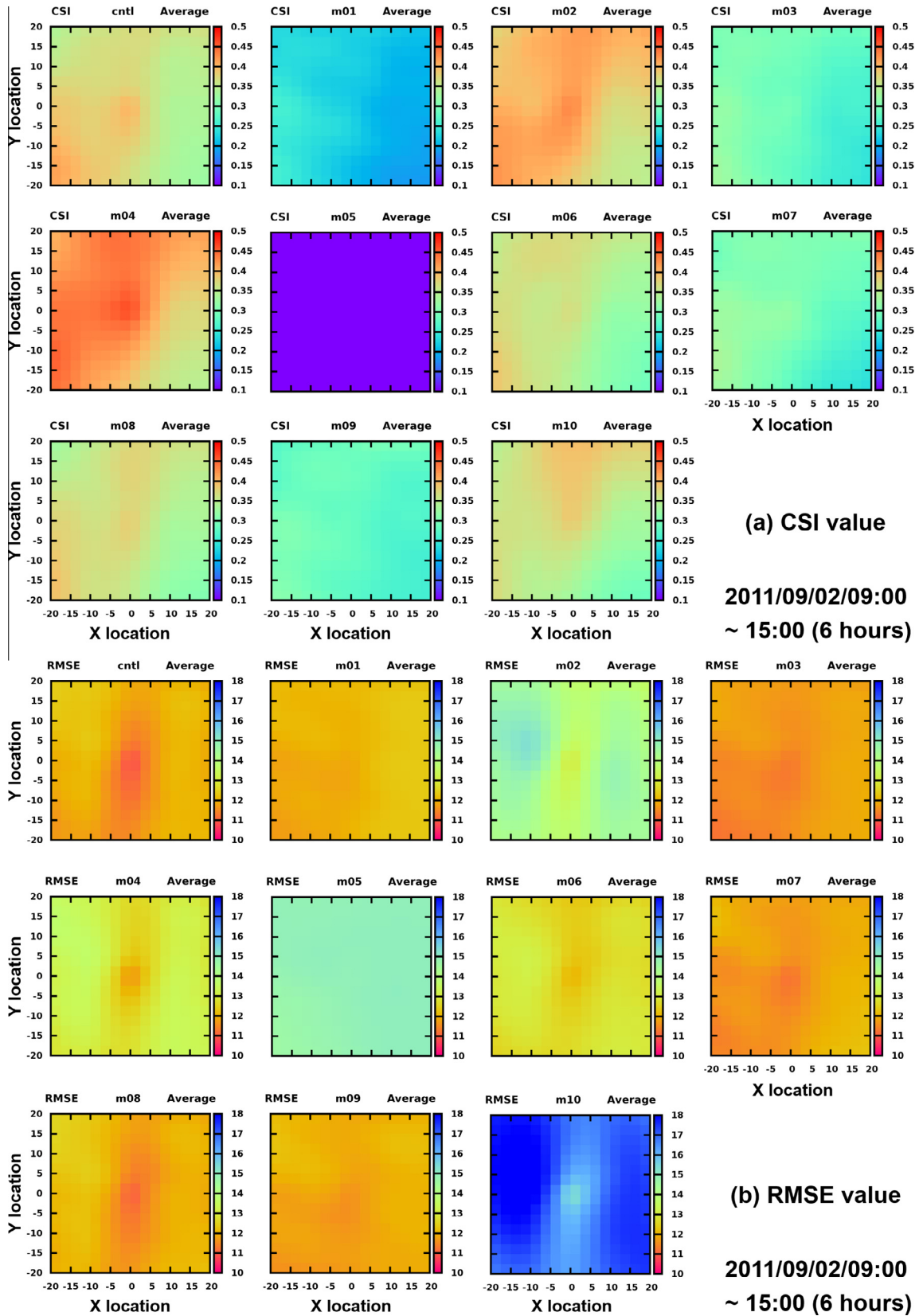


Fig. 10. Same as Fig. 9, but during the period after 6 h (From 0900 JST 2 September to 1500 JST 3 September 2011).

ensemble range (gray range), the ensemble mean (blue curve) of updated ensemble flood forecasting by proposed transposition method, the average result of original NWP ensembles without

the transposition correction (black curve) and observed discharge data of catchment outlet point (red point) for Futatsuno dam catchment.

**Table 3**

Continuity assessment of transposition behaviors of rainfall distribution using correlation coefficients in each 6-h update step.

Period		CC
1st forecast	0–6 h with 6–12 h	0.949
	6–12 h with 12–18 h	0.531
	12–18 h with 18–24 h	0.829
	18–24 h with 24–30 h	0.418
2nd Forecast	0–6 h with 6–12 h	0.504
	6–12 h with 12–18 h	0.619
	12–18 h with 18–24 h	0.842
	18–24 h with 24–30 h	0.834

At first, in the original NWP flood forecasting of the 1st forecast period (rising limb period, left side of Fig. 11), the ensemble spread of the original ensemble forecasting provided a well-matched hydrograph temporal pattern during 0–18 lead times, which were lower and less predictable than the true value from 18 to 30 lead times over the Futatsuno dam catchment; this was caused by an underestimation of the rainfall forecast. After updating using the transposition scheme, the ensemble mean from the proposed method could improve the accuracy of flood forecasting compared to average values of original ensemble NWP, and the ensemble

spread of the updated flood forecast is close to peak discharge in the rising limb period and is maintained through the updating, at 6-h intervals, of the transposition information. In the 2nd forecast period (peak discharge period, right side of Fig. 11), the ensemble spread of the original ensemble forecasting could not represent the peak discharge, whereas an additional ensemble spread of updated flood forecasts, using a transposition scheme, provided the accuracy improvement of ensemble mean value and covered the observed discharge in the peak discharge period.

We also used the index to evaluate accuracy improvement with the results of the original ensemble flood forecasts and post-flood forecasting using the RMSE, which is a quantity used to measure how close each forecast was to the observation. Table 4 shows the RMSE comparisons of ensemble mean value from updated flood forecasting by transposition method with original NWP flood forecasting after 6, 12, 18, and 24 h from start point of original NWP in first and second forecast periods over the Futatsuno and Nanairo dam catchment. As Table 4 shows, our newly proposed method for real-time flood forecast updating could enhance the accuracy of post-flood forecasts with a 6-h update interval, although post-flood forecasting after 24 h in the 1st forecast period over the Nanairo dam catchment indicated a decrease in RMSE accuracy due to a slight over-prediction compared to average val-

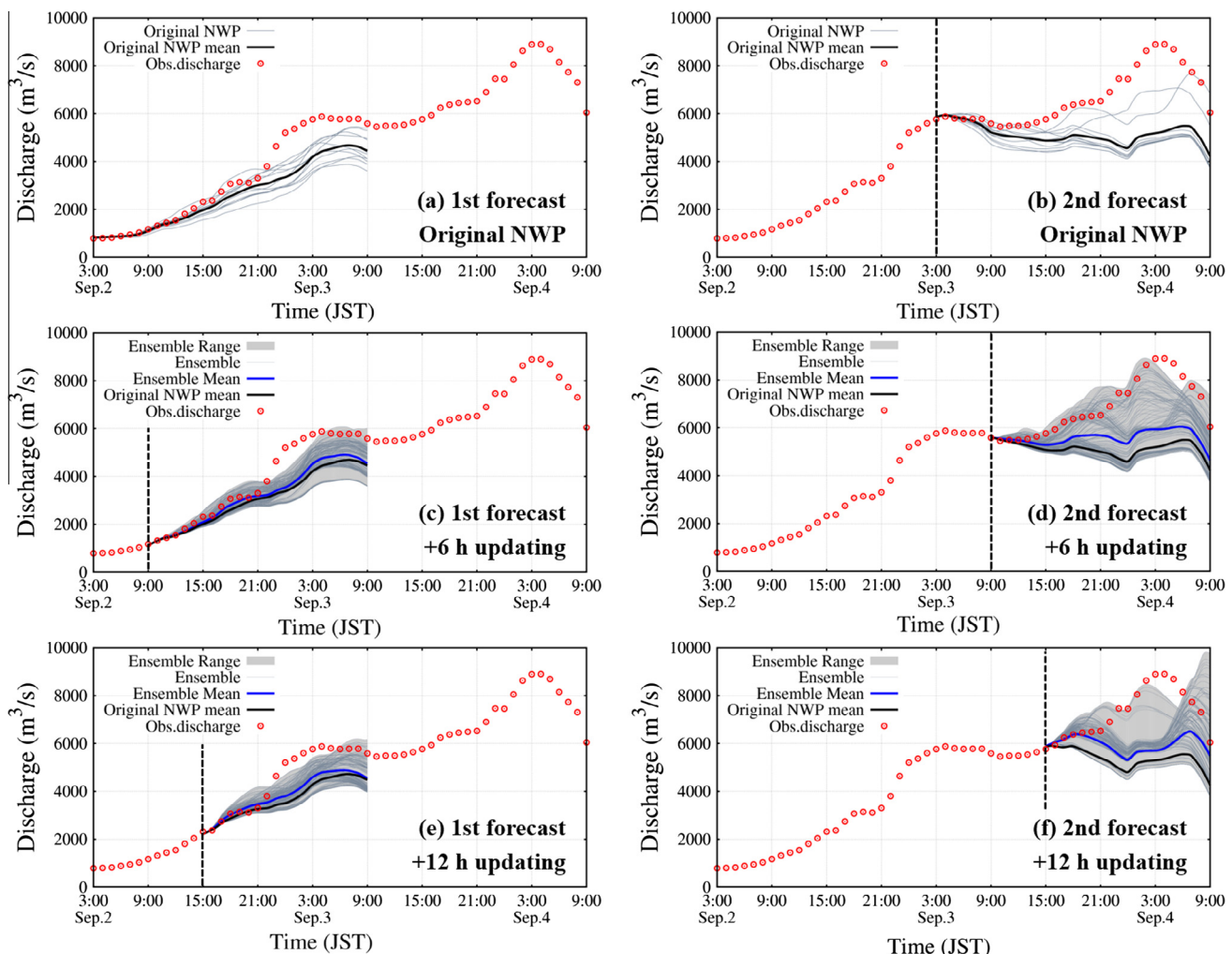


**Fig. 11.** 30 hr flood forecasting using the original 11 ensemble members in 1st and 2nd forecast period (upper; (a) and (b)) and corresponding post-forecasting after 6 h by transposition updating (middle; (c) and (d)) and after 12 h (lower; (e) and (f)) over the Futatsuno dam catchment. Blue line and gray range represent the forecasted discharge of ensemble mean and spread of proposed method, respectively. Black line shows the average result of original NWP ensembles without the transposition updating. Red point represents the observed discharge data of catchment outlet point. (For interpretation of the references to color in this figure legend, the reader is referred to the web version of this article.)

**Table 4**

Comparison of average RMSE of ensemble members for flood forecasting with transposition method and original NWP after 6, 12, 18, and 24 h from start point of original NWP in first and second forecast periods over the Futatsuno and Nanairo dam catchment.

Catchment	Forecast period	Type	From start of original NWP			
			+6 h	+12 h	+18 h	+24 h
Futatsuno	1st	Original NWP	976.3	1047.8	1008.1	272.1
		Proposed method	824.2	860.3	908.0	184.3
	2nd	Original NWP	2117.6	2265.8	2260.7	951.8
		Proposed method	1618.3	1765.8	1670.4	512.2
Nanairo	1st	Original NWP	380.2	424.4	447.5	143.0
		Proposed method	345.4	405.0	388.7	188.0
	2nd	Original NWP	1630.7	1822.1	1783.0	1307.3
		Proposed method	1440.5	1505.7	1328.4	882.6

ues using original ensemble NWP after 24 h, but ensemble spread could cover the observed discharge. From the results of updated post-flood forecasts in Fig. 11 and Table 4, it was shown that QPF location correction using a transposition scheme that considers orographic rainfall could improve the accuracy of flood forecasts, and makes an attractive product for flood forecasting systems with the potential to extend lead time and better quantify predictability.

## 6. Concluding remarks

The Shingu river basin flood on September 2011 in the Kii peninsula, Japan was examined by ensemble rainfall forecasting from NWP model, which are composed of 11 members with a horizontal resolution of 2 km. In previous research of Yu et al. (2013, 2014), flood forecasting patterns from original ensemble 11 members on the small catchment scale are generally similar to observation. However, ensemble mean discharge on peak period is severely under-predicted for most of the ensemble members. In many cases, the time/space scale of the hydrological model is still much finer than that of the meteorological model. Although the NWP-based QPF could generally catch the rainfall pattern, the uncertainties of rainfall to the catchment scale were always significant. And NWP models have challenges with displacement of the forecasting rainband, which means that the intensity and shape of the forecasted storm cell may be correct but the location of the storm cell is wrong.

Given the current issue and problem with EPSs with NWP models, this study aimed to propose an accuracy updating method for flood forecasting using transposition of ensemble rainfall distributions considering orographic effects and to enhance the transposition method proposed in Yu et al. (2014). At first, ensemble forecast rainfalls from the NWP model are separated into orographic and non-orographic rainfall fields using atmospheric variables of GPV data and extraction of the topography effect. Then the non-orographic rainfall fields are shifted by the transposition scheme to produce additional ensemble information and new ensemble rainfall fields are calculated by recombining the transposition results of non-orographic rainfall fields with separated orographic rainfall. Then, the additional ensemble information is applied into a hydrologic model for post-flood forecasting with a 6-h interval. The proposed transposition scheme considering orographic rainfall was verified through largest rainfall event on September 2011, and was applied to the real-time updating of the flood forecasting on two sub-catchments, which are Futatsuno ( $356.1 \text{ km}^2$ ) and Nanairo ( $182.1 \text{ km}^2$ ) dam catchments.

The results of this study lead to the following conclusions:

(1) Orographic rainfall was dominant in the Shingu river basin, which is located in a mountainous region; the percentage of orographic rainfall in the verification area exceeded 50% and its maximum proportion of total rainfall is 99.8%. It

means that the orographic and non-orographic rainfall should be separated and just only non-orographic rain fields should be utilized for spatial transposition.

- (2) From the continuity assessment of transposition behaviors of forecasted rainfall distribution using a correlation coefficient in each 6-h update step, the transposition scheme is continually satisfied during both update steps and has continuity for misplaced locations in the spatial distribution pattern.
- (3) QPF location correction using a transposition scheme that considers orographic rainfall could enhance the under-predicted part of the original ensemble flood forecast method and improve the accuracy of post-flood forecasting with 6-h update intervals over two catchments, which are Futatsuno and Nanairo dam catchments of Shingu river basin, Japan.

However, our transposition scheme focuses on QPF location error correction considering orographic rainfall but not predicted bias correction, which is a quantitative correction that uses the difference between observed and predicted rainfall. For this reason, it is possible to be vulnerable when forecasted rainfall intensity is under-predicted and suitable spatial distribution fails compared with observed reference data. Therefore, bias correction and/or hybrid products with radar-based prediction are required to achieve more reliable hydrologic predictions; bias correction and blending method for accuracy improvement was addressed in Yu et al. (2015). Moreover, we need further research to assess whether the suggested methodology could enhance the accuracy to other flood events.

## Acknowledgement

This study was partly supported by the sub-project of the field 3 on Next Generation Supercomputer Project, 'Prediction of heavy rainfalls by a cloud-resolving NWP system', and was based on data from the Ministry of Land, Infrastructure, Transport and Tourism (MLIT) and J-POWER CO. Ltd. I am grateful for their support.

## References

- Bader, M.J., Roach, W.T., 1977. Orographic rainfall in warm sectors of depressions. *Q. J. R. Meteorol. Soc.* 103 (436), 269–280. <http://dx.doi.org/10.1002/qj.49710343605>.
- Banta, R.M., 1990. The role of mountain flows in making clouds. In: Blumen, W., ed. *Atmospheric Processes over Complex Terrain*: Boston, Massachusetts, American Meteorological Society, Meteorological Monographs, vol. 23(45), pp. 229–283.
- Buizza, R., Miller, M., Palmer, T.N., 1999. Stochastic representation of model uncertainties in the ECMWF ensemble prediction system. *Q. J. R. Meteorol. Soc.* 125, 2887–2908. <http://dx.doi.org/10.1002/qj.49712556006>.
- Buizza, R., Houtekamer, P.L., Toth, Z., Pellerin, G., Wei, M., Zhu, Y., 2005. A comparison of the ECMWF, MSC, and NCEP global ensemble prediction systems. *Mon. Wea. Rev.* 133 (5), 1076–1097. <http://dx.doi.org/10.1175/MWR2905.1>.

- Croke, H.L., Pappenberger, F., 2009. Ensemble flood forecasting: a review. *J. Hydrol.* 375, 613–626. <http://dx.doi.org/10.1016/j.jhydrol.2009.06.005>.
- Cuo, L., Pagano, T.C., Wang, Q.J., 2011. A review of quantitative precipitation forecasts and their use in short- to medium-range streamflow forecasting. *J. Hydrometeorol.* 12, 713–728. <http://dx.doi.org/10.1175/2011JHM1347.1>.
- Demeritt, D., Cloke, H., Pappenberger, F., Thielen, J., Bartholmes, J., Ramos, M.H., 2007. Ensemble predictions and perceptions of risk, uncertainty, and error in flood forecasting. *Environ. Hazards* 7 (2), 115–127. <http://dx.doi.org/10.1016/j.envhaz.2007.05.001>.
- Ebert, E., McBride, J., 2000. Verification of precipitation in weather systems: determination of systematic errors. *J. Hydrol.* 239, 179–202. [http://dx.doi.org/10.1016/S0022-1694\(00\)00343-7](http://dx.doi.org/10.1016/S0022-1694(00)00343-7).
- Fan, F.M., Collischonn, W., Meller, A., Botelho, L.C.M., 2014. Ensemble streamflow forecasting experiments in a tropical basin: the São Francisco river case study. *J. Hydrol.* 519 (Part D), 2906–2919. <http://dx.doi.org/10.1016/j.jhydrol.2014.04.038>.
- Gneiting, T., Raftery, A.E., 2005. Weather forecasting with ensemble methods. *Science* 310, 248–249. <http://dx.doi.org/10.1126/science.1115255>.
- Golding, B.W., 2009. Review – long lead time flood warnings: reality or fantasy? *Meteorol. Appl.* 16, 3–12. <http://dx.doi.org/10.1002/met.123>.
- Hill, F.F., Browning, K.A., Bader, M.J., 1981. Radar and raingauge observations of orographic rain over south Wales. *Q. J. R. Meteorol. Soc.* 107 (453), 643–670. <http://dx.doi.org/10.1002/qj.49710745312>.
- Hlavcová, K., Szolgay, J., Kubík, R., Kohnová, S., Zvolenský, M., 2006. Routing of numerical weather predictions through a rainfall-runoff model. In: Marsalek, J., Stancalík, G., Balint, G. (Eds.), *Transboundary Floods: Reducing Risks through Flood Management*. Springer, NATO Science Series, Dordrecht, Netherlands, pp. 57–68.
- Honda, Y., Sawada, K., 2008. A new 4D-Var for mesoscale analysis at the Japan meteorological agency. *CAS/JSC WGNE, Res. Act. Atmos. Ocea. Model.* 38, 01.7–01.8.
- Houze, R. Jr., 2012. *Cloud Dynamics*. 2nd ed., 496pp.
- Kim, S., Tachikawa, Y., Sayama, T., Takara, K., 2009. Ensemble flood forecasting with stochastic radar image extrapolation and a distributed hydrologic model. *Hydrol. Process.* 23, 597–611. <http://dx.doi.org/10.1002/hyp.7188>.
- Lee, G., Yu, W., Jung, K., Apip, 2013. Catchment-scale soil erosion and sediment yield simulation using a spatially distributed erosion model. *Environ. Earth. Sci.* 70, 33–47. <http://dx.doi.org/10.1007/s12665-012-2101-5>.
- Legg, T.P., Mylne, K.R., 2004. Early warnings of severe weather from ensemble forecast information. *Weather Forecast.* 18, 891–906. [http://dx.doi.org/10.1175/1520-0434\(2004\)019<0891:EWOSWF>2.0.CO;2](http://dx.doi.org/10.1175/1520-0434(2004)019<0891:EWOSWF>2.0.CO;2).
- Lin, Y.L., Farley, R.D., Orville, H.D., 1983. Bulk parameterization of the snow field in a cloud model. *J. Appl. Meteorol.* 22, 1065–1092. [http://dx.doi.org/10.1175/1520-0450\(1983\)022<1065:BPOTSF>2.0.CO;2](http://dx.doi.org/10.1175/1520-0450(1983)022<1065:BPOTSF>2.0.CO;2).
- Lorenz, E., 1969. The predictability of a flow which contains many scales of motion. *Tellus A* 21, 289–307.
- Nakakita, E., Ikebuchi, S., Nakamura, T., Kanmuri, M., Okuda, M., Yamaji, A., Takasao, T., 1996. Short-term rainfall prediction method using a volume scanning radar and GPV data from numerical weather prediction. *J. Geophys. Res.* 101 (D21), 26181–26197.
- Nakakita, E., Terazono, M., 2008. Short-term rainfall prediction taking into consideration nonlinear effect of non-orographic rainfall on orographic rainfall. *Ann. J. Hydraul. Eng. Jpn Soc. Civil Eng. (JSCE)* 52, 331–336 (in Japanese with English abstract).
- Nakakita, E., Yoshikai, T., Kim, S., 2012. Application of error-ensemble prediction method to a short-term rainfall prediction model considering orographic rainfall. *IAHS Publ. Proceedings of 2011 International Weather Radar and Hydrology symposium, Exeter, UK*, vol. 351, pp. 311–316.
- Noh, S.J., Rakovec, O., Weerts, A.H., Tachikawa, Y., 2014. On noise specification in data assimilation schemes for improved flood forecasting using distributed hydrological models. *J. Hydrol.* 519 (Part D), 2707–2721. <http://dx.doi.org/10.1016/j.jhydrol.2014.07.049>.
- Palmer, T.N., 2002. The economic value of ensemble forecasts as a tool for risk assessment: from days to decades. *Quart. J. Roy. Meteorol. Soc.* 128, 147–174. <http://dx.doi.org/10.1256/0035900021643593>.
- Palmer, T., Buizza, R., 2007. Fifteenth anniversary of EPS. *ECMWF Newsletter* 114, 14p.
- Roe, G.H., 2005. Orographic precipitation. *Annu. Rev. Earth Planet. Sci.* 33, 645–671. <http://dx.doi.org/10.1146/annurev.earth.33.092203.122541>.
- Robichaud, A., Austin, G.L., 1988. On the modelling of warm orographic rain by the 'seeder-feeder' effect. *Q. J. R. Meteorol. Soc.* 114 (482), 967–988. <http://dx.doi.org/10.1002/qj.49711448207>.
- Roulin, E., Vannitsem, S., 2005. Skill of medium-range hydrological ensemble predictions. *J. Hydrometeorol.* 6 (5), 729–744. <http://dx.doi.org/10.1175/JHM436.1>.
- Saito, K., Fujita, T., Yamada, Y., Ishida, J., Kumagai, Y., Aranami, K., Ohmori, S., Nagasawa, R., Kumagai, S., Muroi, C., Kato, T., Eito, H., Yamazaki, Y., 2006. The operational JMA nonhydrostatic meso-scale model. *Mon. Wea. Rev.* 134, 1266–1298. <http://dx.doi.org/10.1175/MWR3120.1>.
- Saito, K., 2012. The JMA nonhydrostatic model and its application to operation and research. In: Yucel, I. (Ed.), *Atmospheric Model Applications*. InTech, pp. 85–110. Available online at <http://cdn.intechopen.com/pdfs-wm/34744.pdf>.
- Sayama, T., Tachikawa, Y., Takara, K., Ichikawa, Y., 2006. Development of a real-time distributed flood prediction system in a flow regulated river basin. In: *Proc. of the 3rd APHW Conference on "Wise Water Resources Management towards Sustainable Growth and Poverty Reduction"*.
- Schaake, J., Perica, S., Mullusky, M., Demargne, J., Welles, E., Wu, L., 2004. Pre-processing of atmospheric forcing for ensemble runoff prediction. In: *Proceedings of the 84th AMS Annual Meeting*. Available at <http://ams.confex.com/ams/pdffiles/72172.pdf>.
- Smith, R.B., 1979. The influence of mountains on the atmosphere. *Adv. Geophys.* 21, 87–230. [http://dx.doi.org/10.1016/S0065-2687\(08\)60262-9](http://dx.doi.org/10.1016/S0065-2687(08)60262-9).
- Smith, R.B., 2006. Progress on the theory of orographic precipitation. *Special Paper 398: Tectonics, Climate, and Landscape Evolution*, S. D. Willett et al., Eds., Geological Society of America, pp. 1–16. [http://dx.doi.org/10.1130/2006.2398\(01\)](http://dx.doi.org/10.1130/2006.2398(01)).
- Smith, R.B., Schafer, P., Kirshbaum, D.J., Regina, E., 2008. Orographic precipitation in the Tropics: experiments in Dominica. *J. Atmos. Sci.* 66, 1698–1716. <http://dx.doi.org/10.1175/2008AS2920.1>.
- Seo, D.-J., Liu, Y., Moradkhani, H., Weerts, A., 2014. Ensemble prediction and data assimilation for operational hydrology. *J. Hydrol.* 519 (Part D), 2661–2662. <http://dx.doi.org/10.1016/j.jhydrol.2014.11.035>.
- Tachikawa, Y., Nagatani, G., Takara, K., 2004. Development of stage-discharge relationship equation incorporating saturated–unsaturated flow mechanism. *Ann. J. Hydraul. Eng. JSCE* 48, 7–12 (in Japanese with English abstract).
- Tatehira, R., 1976. Orographic rainfall computation including cloud–precipitation interaction. *Tenki* 23, 95–100 (in Japanese).
- Xuan, Y., Cluckie, I., Wang, Y., 2009. Uncertainty analysis of hydrological ensemble forecasts in a distributed model utilizing short-range rainfall prediction. *Hydrol. Earth Syst. Sci.* 13, 293–303. <http://dx.doi.org/10.5194/hess-13-293-2009>.
- Yu, W., Nakakita, E., Yamaguchi, K., 2013. Assessment of probabilistic flood Forecasting using ensemble NWP rainfall with 30hr forecast time during typhoon events. *Adv River Eng. JSCE* 19, 235–240.
- Yu, W., Nakakita, E., Kim, S., Yamaguchi, K., 2014. Accuracy improvement of flood forecasting using pre-processing of ensemble numerical weather prediction rainfall fields. *Journal of Japan Society of Civil Engineers, Ser. B1 (Hydraulic Engineering)* 70, L-151–L-156.
- Yu, W., Nakakita, E., Kim, S., Yamaguchi, K., 2015. Improvement of rainfall and flood forecasts by blending ensemble NWP rainfall with radar prediction considering orographic rainfall. *J. Hydrol.* 531 (Part 2), 494–507. <http://dx.doi.org/10.1016/j.jhydrol.2015.04.055>.